Energy harvesting from a magnetic levitation system

Energy harvesting from a magnetic levitation system

Krzysztof Kecik[a,*], Andrzej Mitura[a], Stefano Lenci[b], Jerzy Warminski[a]

[a] *Lublin University of Technology,Department of Applied Mechanics, Nadbystrzycka 36 Street, 20-618 Lublin, Poland*
[b] *Department of Civil and Building Engineering, and Architecture, Polytechnic University of Marche, via Brecce Bianche, 60131 Ancona, Italy*

Abstract

Numerical and experimental studies of a magnetic levitation harvester are presented in the paper. The idea is based on the motion of permanent cylinder magnet in a coil exploited for energy harvesting. The novel model is based on a new definition of the coupling coefficient (inductive coefficient) which relates mechanical and an electrical components. The performed static and dynamics experimental tests show that this coefficient is a nonlinear function of the magnet position, and highly depends on the magnet coordinate in the coil, in such a way that the maximum energy is obtained in a coil ends. The comparison between classical – fixed value model – and novel nonlinear model of the inductive coefficient is presented for selected cases. The most essential differences are presented.

Keywords: `magnetic levitation, energy harvesting, coupling coefficient, experimental identification.`

1. Introduction

Energy harvesting (EH), also called energy scavenging (ES), is the process of transforming ambient energy into useful electrical energy. In the last decade, energy harvesting has received growing attention. This is due to the power reduced

*Corresponding author
Email addresses: `k.kecik@pollub.pl` (Krzysztof Kecik), `a.mitura@pollub.pl` (Andrzej Mitura), `lenci@univpm.it` (Stefano Lenci), `j.warminski@pollub.pl` (Jerzy Warminski)

requirement of small electronic devices and wireless transmission. Usually, the energy is harvested from ambient resources such as: wind, solar radiation, thermal resources, and vibrations (motions). Among these resources, the vibration energy harvesters are widely used, because vibrations are the most attractive source for energy recovery purposes. The vibrational energy harvester systems require a mechanism that transfers a mechanical energy into the electrical one. The most popular method of transferring energy in vibration harvesters are: electromagnetic, piezoelectric, electrostatic and magnetostrictive. The electromagnetic energy harvesters (EMEHs) are based on the Faradays law of electromagnetic induction, and then usually the device has coil-magnet components [1]. The piezoelectric energy harvesters (PEHs) use mechanical strain to energy recovery [2]. The electrostatic energy harvesters (ESEHs) use capacitors to transfer mechanical into the electrical energy [3]. The magnetostrictive energy harvesting (MEH) is based on the vibration which change magnetization and on a magnetostrictive material that produces a magnetic field while deformed [4]. Generally, electromagnetic, electrostatic and piezoelectric are the three common vibration energy harvesting mechanisms.

The magnetic induction harvester is one of the earliest applied systems for energy harvesting and this type of device is studied in this work. These harvesters can be classified on the base of the mechanism they exploit to achieve a relative velocity between the coil and the magnet, linear [5] or rotational motion [6, 7]. The recovered energy depends on the motion between the coil and magnet, which changes the magnetic flux and then voltage is induced. The magnitude of harvested energy can range up to kilowatts, although this highly dependents on the size of the device [8]. A cantilever beam energy harvester with a magnetic restoration forces used to create required behavior is presented in [9]. The high energy was applied to extend a bandwidth of the device. Joyce [10] proposed an electromagnetic energy harvester consisting of a magnet mounted inside a tube with coils. This system is dedicated to monitor the structural health of large wind turbines. The rotating turbine blades caused the magnet sliding along the tube and the voltage – required to structural health monitoring system – was

recovered.

One of the most interesting electromagnetic harvester, so called 'maglev' is based on the levitation phenomenon. The maglev harvesters are characterized by their simplicity, lack of dampers and springs. Additionally, they ensure a high reliability in work. Mann and Sims [11] proposed a simple magnetic levitation harvester. The suspension of this device consist of two outer magnets which were orientated such that their poles were repelling the third levitated middle magnet. They showed that the resulting magnetic restoring force could be accurately described by a cubic nonlinearity spring characteristic, similar to the hardening spring Duffing oscillator. However, they assumed the inductive coefficient, coupling mechanical and magneto-electrical fields, as fixed. The analytical and semi-analytical study of nonlinear magnetic levitation-based models dedicated for energy harvesting is shown in papers [12, 13, 14]. However, again the coupling coefficient was considered as constant.

In the paper present paper a new model for the coupling coefficient is proposed. It is identified on the basis of experimental quasi-static and dynamic tests, and it describes the relationship between inductive coefficient and the magnet's position. This is in contrast to the literature where in many papers, the coupling coefficient is assumed to be constant dependent on the construction of the coil [11, 15, 16, 17, 18]. That approach may lead to inaccurate results.

2. Harvester Maglev System

2.1. Motivation

The motivation of this our work is a research project dealing with the vibration mitigation and energy recovery. In the study, a special laboratory harvester-absorber system based on magnetic levitation (maglev) phenomenon mounted in the vibration absorber (a pendulum) has been built. The photo of a laboratory rig is shown in Fig.1. The system allows to simultaneously reduce vibration and recover the energy. More information about this apparatus can be found in [19].

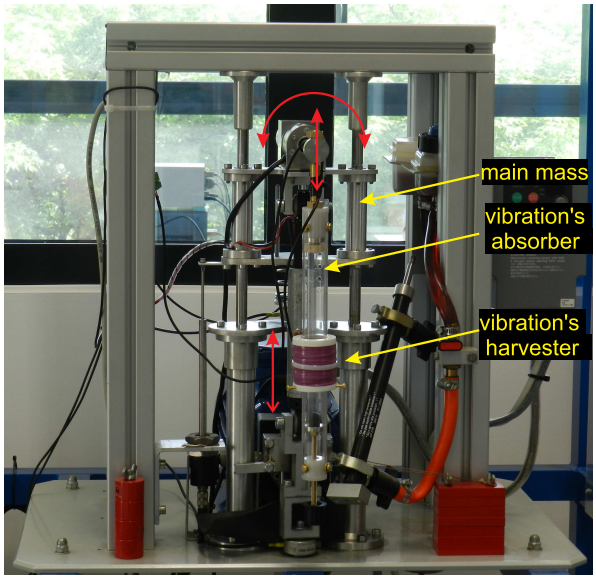

Figure 1: The experimental harvester-absorber system.

The electromagnetic induction of a voltage in a coil caused by motion of the magnet is one of fundamental problems in physical phenomena. Therefore, the proper description of the coupling inductive coefficient is a crucial problem from harvesting point of view. Usually, in the literature the coupling of the electromagnetic and the mechanical systems are described as a constant coefficient. However, if the fixed value of the coefficient is not properly identified, especially for large vibrations of the magnet, this simplification can lead to imprecise results. Therefore, the identification of a function which describes the coupling coefficient, based on static and dynamics experimental tests, is the main goal of this paper.

2.2. Description of maglev element

The maglev component of the harvester is a crucial element of the laboratory rig, presented in Fig.1. Therefore, in this paper, only the maglev system is studied. The magnetic levitation harvester consists of a cylindrical non-magnetic tube (made of plexiglass material) with two cylindrical permanent

magnets (top and bottom) mounted inside tube on ends. The third magnet (moving) oscillates in the tube between the fixed magnets and experiences a levitation force coming from each pair of magnets having magnetic poles oriented to repel i.e. $S-S$, $N-N$). The coil is formed by winding wire around the outer surface of the tube. To eliminate the air compressibility problem, special holes on the surface tube were made. The photo of the maglev system is shown in Fig. 2(a), while the scheme of the electromagnetic harvester device is presented in Fig.2(b). The moving magnet can oscillate under the excitation of the base vibrations $y(t)$ and then the electromotive forces (EMF) in a coil mounted on the tube is induced.

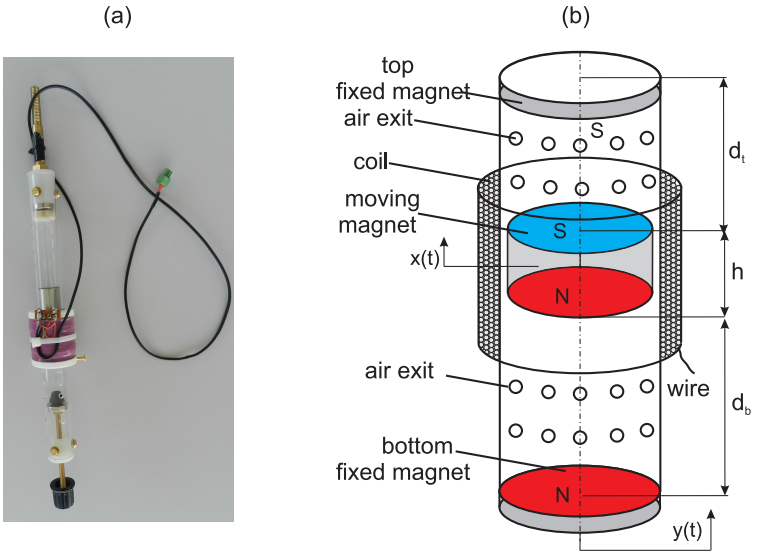

Figure 2: The maglev system: a real view (a) and scheme (b).

The magnetic restoring force characteristic is described with help of the simple static displacement test. The magnetic levitation force is calibrated by measurement the displacement between the moving and the bottom magnets (distance d_b, in Fig. 2(b)) for various masses of the moving magnet. A series of experimental measurements is presented in Fig. 3(a) where the force against a separation distance between the magnets d_b is plotted. The characteristic from Fig. 3(a) is then transformed into the x coordinate which represents the

distance of the moving magnet from the static equilibrium point (Fig.3(b)).

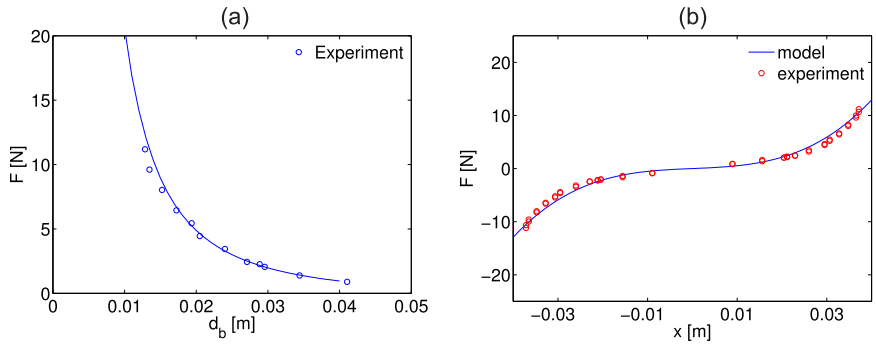

Figure 3: The levitation force plotted (a) as a static function of the separation distance between the moving and bottom magnet and (b) a force-displacement model magnetic suspension (a hard Duffing characteristic). Distance between permanent magnets $40mm$.

On the basis of this result a model of the complete magnetic suspension is developed. The total restoring force is calculated as sum of two restoring forces. Because the top and bottom magnets are the same, we assume the levitation forces between the top and moving magnet as well bottom and moving magnet are identical. The comparison between the experiment results and the adopted force-displacement model is shown in Fig.3(b). The mathematical model has a form of monostable hard Duffing characteristics $kx + k_1x^3$, Fig.3(b). For the tested experimental setup the stiffness coefficients take values: $k = 35$ [N/m], $k_1 = 180000[\mathrm{N/m^3}]$. A similar suspension model of the magnetic levitation effect is proposed by Mann and Sims [11]. Note, that the suspension parameters of the model highly depends on the distance between permanent magnets. Therefore, a change of this distance causes essential change in the characteristic.

2.3. Electromechanical harvester

The electromechanical model of the considered harvester is presented in Fig.4(a). The levitation restoring force (represented by a spring) is modelled by hard Duffing characteristics with linear k and non-linear k_1 stiffness components. Mass of the moving magnet is defined as m, while the mechanical viscous damping is defined by the c coefficient. The displacement of the middle magnet

measured from its static equilibrium position is represented by coordinate $x(t)$, whereas the displacement of the base $y(t)$ is the excitation, which in the present work is assumed to be harmonic, $y(t) = A\sin(\omega t)$.

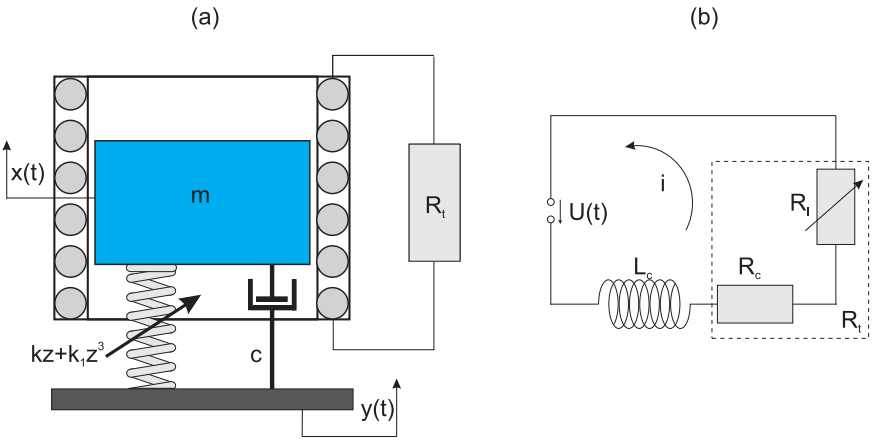

Figure 4: The electromechanical harvester model (a) and electrical circuit (b).

The electrical circuit of the harvester is shown in Fig.4(b). It consists of a coil with inductance L_c and resistance R_c. The coil is connected to the load resistor (R_l). This resistance can be varied in a range of $0 - 10k\Omega$. The sum of the coil and load resistances is named as total resistance (R_t). During oscillations of the moving magnet, the current i and voltage U are induced.

Introducing of the relative magnet's displacement $z(t) = x(t) - y(t)$, the governing equations of motion for this system have the form (g is the gravity field, assumed to act in the $-x$ direction).

$$m\ddot{z} + c\dot{z} + kz + k_1 z^3 + \alpha(z)i + mg = -m\ddot{y}, \tag{1}$$

$$L_c\dot{i} + R_t i = \alpha(z)\dot{z}. \tag{2}$$

The parameter $\alpha(z)$ is the coupling coefficient which is the crucial point of the model and is described in the next section. Usually, in the literature, these equations are simplified. For vibrations with a small amplitude, the non-linearity defined by coefficients k_1 is neglected, the parameter α is assumed as constant, and the harvester is treated as linear[20].

2.4. Coupling coefficient

A proper definition of the coupling coefficient is a crucial problem from modelling point of view. This parameter characterizes how the induced voltage in the coil is related to the velocity of the magnet. In the literature, multiple approaches in order to determine the coupling term can be found. The most common method have treated the magnetic flux density as uniform over the coil range of motion (average) [16, 17, 18, 21, 22]. This assumption leads to a coupling factor which has a fixed value, and strongly simplifies the analysis of the energy harvester. The second method is an experimental determination of α as a function of the magnet's position. Usually, this approach is applied for the complicated harvesters [23] but again a constant coupling coefficient is sought. In some papers the coupling factor has been evaluated using the finite element approach [24],[25].

The coupling coefficient α highly depends on the magnet's position. In order to determine it experimentally the Eq.(2) is modified into the form:

$$\alpha(z) = \frac{L_c\dot{i} + R_t i}{\dot{z}}. \tag{3}$$

The signals i and $\dot{z}$ were measured during the experiment tests. The time derivative $\dot{i}$ was numerically calculated, as the first derivative of signal i. In α estimation, the coil inductance L_c parameter was included. However, the influence of the inductance is much smaller then resistance R_t which is about 1600 times larger.

Figure 5 shows a plot of the quasi-static (red) and the dynamic (blue) tests of the coupling coefficient. The static test has been performed with the constant velocity equals $v = 0.016\,[\mathsf{m/s}]$ in positive and then negative directions. It means that the magnet was moved by a triangular signal. The maximal value of α is reached close to the ends of the coil ($\alpha \approx 60\,[\mathsf{Vs/m}]$, for $x = -0.02\,[\mathsf{m}]$ and $x = 0.02\,[\mathsf{m}]$).

In the dynamic test, the magnet was exited by the periodic signal with velocity defined by: $v(t) = v_{max}\sin(2\pi f t)$, where $f = 0.28\,[\mathsf{Hz}]$ is the frequency and the maximum speed is $v_{max} = 0.195\,[\mathsf{m/s}]$. This characteristic (blue line in Fig.5)

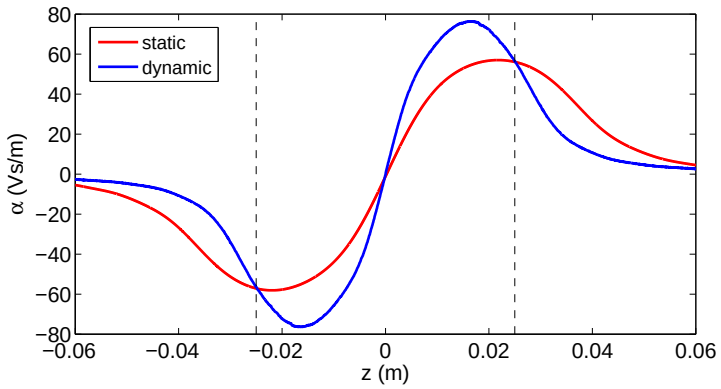

Figure 5: The coupling coefficient determined by the quasi-static test with velocity $v = 0.016\,[\mathrm{m/s}]$ (red line) and by the dynamic test with $v_{max} = 0.195\,[\mathrm{m/s}]$ (blue line).

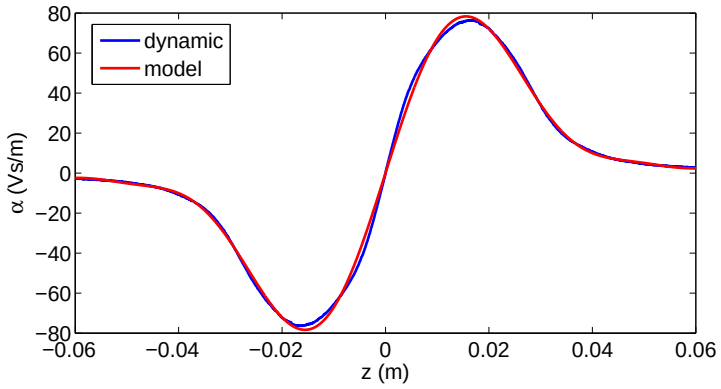

Figure 6: The proposed polynomial model (red) compared with the dynamic coupling coefficient (blue).

shows that maximal value of α appears for $z = -0.018\,[\mathrm{m}]$ and $z = 0.018\,[\mathrm{m}]$, and equals $\alpha \approx 80\,[\mathrm{Vs/m}]$.

It is worth to underline that both the static and the dynamic tests provide the same qualitative behaviour for the curve $\alpha(z)$. The differences are only quantitative, and come from the dynamics of the electrical circuit, due to dynamic changes of the periodically varied signal. Note, that both tests were performed for $y(t) = 0$, therefore $z(t) = x(t)$. The static and dynamic tests have been per-

formed for selected velocity of the magnet, being within the range of the velocity occurring in the laboratory system shown in Fig. 1. For these parameters, the coil inductance and the total resistance practically do not influence the model coupling coefficient.

As we have seen, α is far from constant, but indeed it is a *nonlinear* function of the magnet position. The experimental curve $\alpha(z)$ has a complex expression. Thus, for its use in the model equations (1) and (2), a polynomial approximation is proposed, which is easier to be implemented. It is determined by a least squares curve-fitting technique, and has a form of odd polynomial function of thirteenth degree

$$\alpha(z) = a_1 z + a_2 z^3 + a_3 z^5 + a_4 z^7 + a_5 z^9 + a_6 z^{11} + a_7 z^{13}. \tag{4}$$

The parameters of this polynomial are: $a_1 = 8.1594e{+}03[\mathsf{Vs/m}^2], a_2 = -1.5686e{+}07[\mathsf{Vs/m}^4], a_3 = 1.2748e{+}10[\mathsf{Vs/m}^6], a_4 = -5.4551e{+}12[\mathsf{Vs/m}^8], a_5 = 1.2841e{+}15\ [\mathsf{Vs/m}^{10}], a_6 = -1.5719e+17\ [\mathsf{Vs/m}^{12}], a_7 = 7.8157e+18\ [\mathsf{Vs/m}^{14}]$. This experimentally-based definition of the coupling coefficient is presented in Fig. 6 and it is used for the further numerical analysis and comparison with the existing models.

The model coupling coefficient has been determined for harmonic excitation, which allows to work the harvester together with moving harmonically a pendulum-like dynamic absorber.

3. Numerical Analysis

The comparison of the new proposed polynomial model with classical approach is the main goal of this analysis. The values of parameters are taken from the experimental rig: $m = 0.098\,[\mathsf{kg}], k = 35\,[\mathsf{N/m}], k_1 = 180000\,[\mathsf{N/m}^3], c = 0.054\ [\mathsf{Ns/m}], L_c = 1.46\ [\mathsf{H}], R_t = 2300\ [\Omega]$ and $A = 0.01\ [\mathsf{m}]$. All calculations are performed with Auto07p [26], for the continuation method, and in Matlab 2015, for direct numerical simulations.

The resonance curves for the magnet's displacement (z), the velocity ($\dot{z}$) as well as the recovered current (i) versus frequency of excitation ω are shown

in Figs.7−9 respectively. The numerical calculation have been performed for varying frequency ω and for fixed displacement amplitude $A = 0.01\,[\mathsf{m}]$, so that the amplitude of excitation force which is $mA\omega^2$, changes along the resonance curves.

The figures on the left side Figs. 7(a)-9(a) present results obtained for the classical approach with constant coupling coefficient, while figures on the right side Figs. 7(b)-9(b) show results for the proposed polynomial model (red colour). Three different values of α have been selected, based on Fig.6. In order to compare results we decided to choose small, average and large value of α from function determined in Fig.6. The black line corresponds to the case where the fixed coupling coefficient has smaller value and equals to $\alpha = 5\,[\mathsf{Vs/m}]$, the green line to $\alpha = 30\,[\mathsf{Vs/m}]$ and the blue line to $\alpha = 60\,[\mathsf{Vs/m}]$.

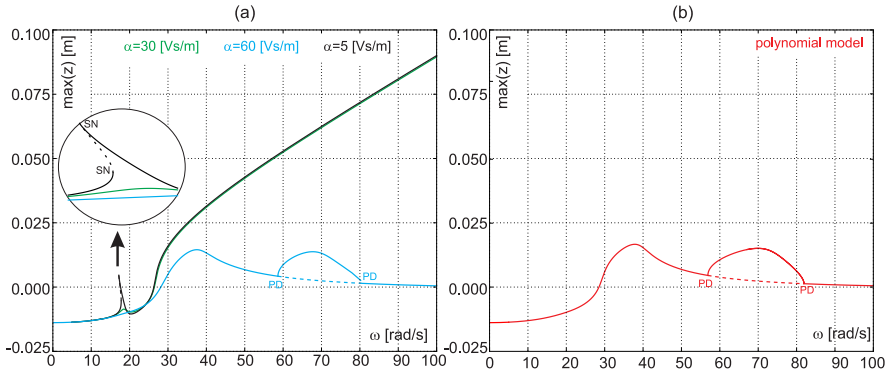

Figure 7: Resonance curves of the magnet's displacement (z), for the fixed (a) and the polynomial (b) coupling coefficient model.

The unstable solutions are marked by dash-dotted lines, while the solid lines denote the stable solutions. The points labelled as SN and PD denote the saddle–node and period doubling bifurcations, respectively. For the small value of α the resonance curves obtained from the classical and proposed model are different. Note, that resonance curves for $\alpha = 5\,[\mathsf{Vs/m}]$ and $\alpha = 30\,[\mathsf{Vs/m}]$ are very similar, with almost overlapped curves. Near, the frequency $\omega = 19\,[\mathsf{rad/s}]$ the first resonance peak is observed. Higher value of α and the proposed polynomial model of α reduced the resonance peak. This denotes, that α plays the

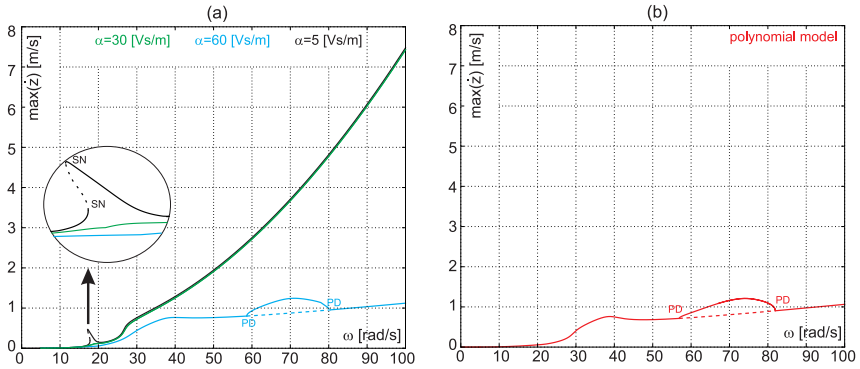

Figure 8: Resonance curves of the magnet's velocity ($\dot{z}$), for fixed (a) and polynomial (b) coupling coefficient.

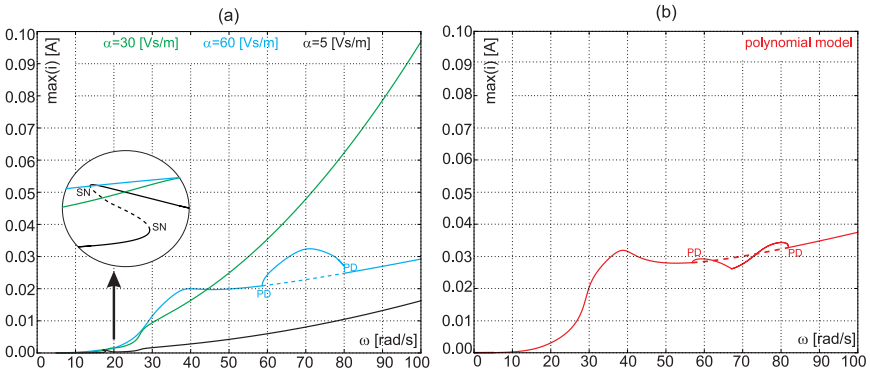

Figure 9: Resonance curves of the recovered current, for fixed (a) and polynomial (b) coupling coefficient.

role of electrical damping. Additionally, for the large vale of α, the obtained resonance curves are similar to the new model (see $\alpha = 60\,[\mathsf{Vs/m}]$ in Fig.6(a) and Fig.6(b)). This means that for large α value, the classical model is close to the improved description of the coupling coefficient. The same situation is observed for the magnet velocity resonance curve (Fig.7(a)-(b)).

Interestingly, in the range $\omega \approx 58 - 82\,[\mathsf{rad/s}]$ the loss of stability by the period doubling bifurcation is observed and motion changes period from T to $2T$. In this region, the maximal current differs essentially while comparing both models. In the proposed model the current can be slightly larger or smaller, depending

on excitation frequency, Fig.9(a) and (b).

Two parameters amplitude–frequency plots (A, ω) presented in Fig.10 show region in which motion with double period of the original orbit exist. In case of the polynomial model this region is slightly different (Fig.10(b)).

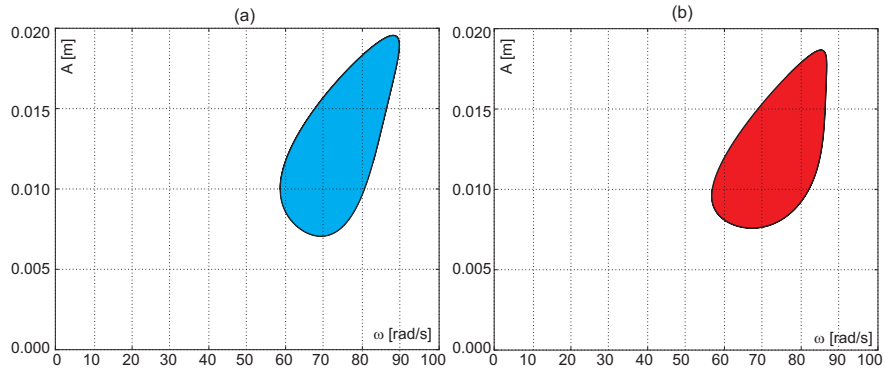

Figure 10: Two parameters space plot shows solution with double period, for fixed $\alpha = 60\,[\mathsf{Vs/m}]$ (a), and the polynomial model's coupling coefficient (b).

In order to have a confirmation of the results obtained by the continuation method, the brute force bifurcation diagrams are determined by direct numerical integrations, using the "following attractor method", namely the initial condition for a parameter value is the final condition for the previous value of the parameter. The first iteration starts from $[z, \dot{z}, i] = [0, 0, 0]$.

For small value of $\alpha = 5\,[\mathsf{Vs/m}]$ the increment of ω shows periodic solution with period T equal to the excitation period, see Fig.11. But, for the decreasing parameter the solution changes its period from T to $2T$ for $\omega \approx 75 \div 90\,[\mathsf{rad/s}]$. Near the natural frequency $\omega = 19\,[\mathsf{rad/s}]$ the first resonance peak appears which agrees with the continuation method (see Fig.7(a)).

Similar situation is observed for $\alpha = 30\,[\mathsf{Vs/m}]$ in Fig.12. In this case however, the period 1 solution is observed for increasing ω (blue line), while for decreasing (black line), starting from $\omega = 100\,[\mathsf{rad/s}]$, the periodic solution with period T, goes to period doubling $2T$, and finally to chaotic motion (for $\omega \approx 65 \div 80\,[\mathsf{rad/s}]$, black area in Fig.12). For frequency smaller then $65\,[\mathsf{rad/s}]$, the solution jumps to periodic and the difference between two integrations is not observed.

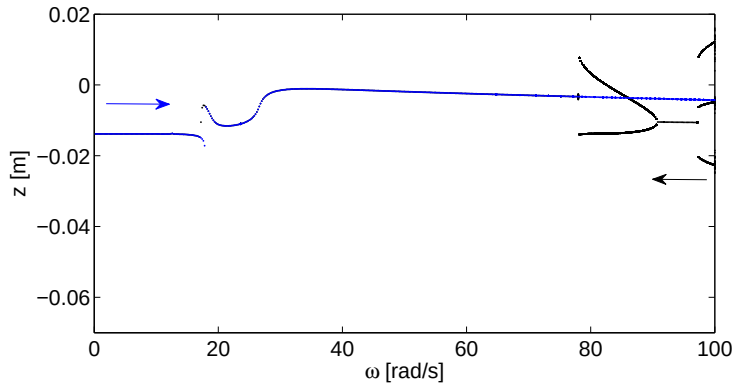

Figure 11: Bifurcation diagram, the magnet's displacement vs. frequency of excitation, for $\alpha = 5\,[\mathsf{Vs/m}], A = 0.01\,[\mathsf{m}]$. The arrows show direction of numerical integration.

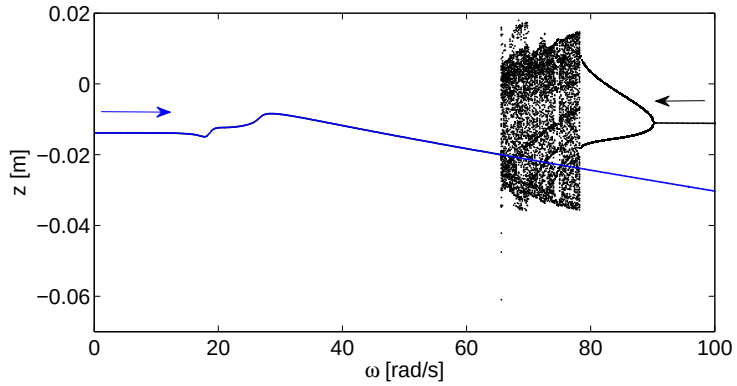

Figure 12: Bifurcation diagram, the magnet's displacement vs. frequency of excitation, for $\alpha = 30\,[\mathsf{Vs/m}], A = 0.01\,[\mathsf{m}]$. The arrows show direction of numerical integration.

The bifurcation diagrams in Fig.13 and Fig.14 are computed, respectively, for larger value of $\alpha = 60\,[\mathsf{Vs/m}]$, and for the polynomial model. The results are very similar between each other but essentially different from the former cases. In both diagrams, the period 1 solution is independent of the direction of the bifurcation parameter variation. Oscillations with double period $2T$ occurs for the frequency domain $\omega \approx 60 \div 85$. This result agrees with the those presented in Figs.9 and 10.

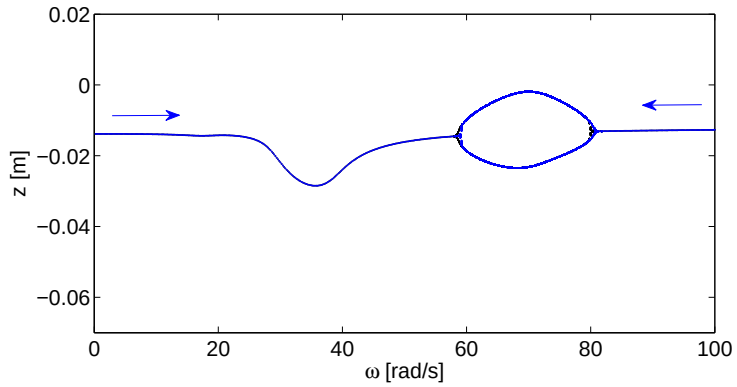

Figure 13: Bifurcation diagram, the magnet's displacement vs. frequency of excitation, for $\alpha = 60\ [\mathsf{Vs/m}], A = 0.01\ [\mathsf{m}]$. The arrows show direction of numerical integration.

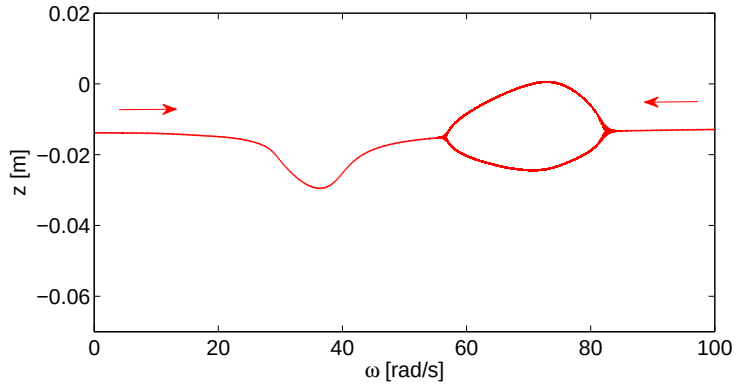

Figure 14: Bifurcation diagram, the magnet's displacement vs. frequency of excitation, for α polynomial model, and $A = 0.01\ [\mathsf{m}]$. The arrows show direction of numerical integration.

The above analysis demonstrates clearly that models with constant coupling parameter α has to be carefully calibrated in order to get realistic solutions. The influence of the coupling coefficient α (for fixed α model) on harvested energy is shown in Fig.15. For small excitation frequency $\omega = 20\ [\mathsf{rad/s}]$ a single solution exists (Fig.15(a)). The maximal recovered current equals about $i = 2.3\ [\mathsf{mA}]$ with plateau around $\alpha \approx 30 \div 70\ [\mathsf{Vs/m}]$.

However, for the higher frequency $\omega = 70\ [\mathsf{rad/s}]$, the constant parameter

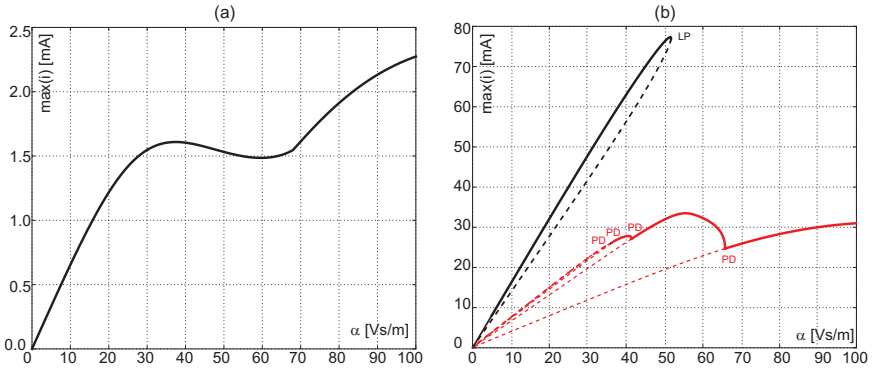

Figure 15: Bifurcation diagrams, the coupling coefficient vs. recovered current (i), for $\omega = 20$ [rad/s] (a) and $\omega = 70$ [rad/s] (b).

model exhibits two independent solutions with different bifurcation scenarios (red and black branches in Fig.15(b)). Therefore, only one solution was observed on the resonance curve presented in (Fig.9(a)), where the calculation was performed by the branch continuation method. The red branch in Fig.15(b)) leads to chaos by a cascade of a period doubling bifurcation.

4. Conclusions and Remarks

The paper presents numerical and experimental analysis of magnetic levitation harvester. The determination of the coupling coefficient, the parameter which couples mechanical and electrical parts, is analysed in detail. In order to get a proper description of this parameter, static and dynamic tests have been performed. On this basis the characteristics of the coupling coefficient versus magnet position were obtained. The detailed experimental tests allowed determination the polynomial model which is a new proposal with respect to the constant coefficient model commonly used in the literature.

The obtained results show, that fixed value of coupling coefficient can be accepted, provided that it is properly chosen. The improper estimation of this parameter may lead to artificial solutions including chaotic motion which do not exists in the real system.

The obtained results show that for the tested device the recovered power reaches about three watts. It is expected that in larger structures the harvested energy will get higher amounts.

The next step in this research will be the development of the analytical method which allows a proper selection the most appropriate fixed value of the coupling coefficient.

Acknowledgement

This work was financially supported under project of National Science Centre according to decision no. DEC-2013/11/D/ST8/03311.

References

[1] J. Liu, S. Garrett, Characterization of a small moving-magnet electrodynamic linear motor, Journal of the Acoustical Society of America 118 (4) (2005) 2289–2294. doi:10.1121/1.2011155.

[2] S. Crossley, S. Kar-Naryan, Energy harvesting performance of piezoelectric ceramic and polymer nanowires, Nanotechnology 26 (34) (2015) 344001. doi:10.1088/0957-4484/26/34/344001.

[3] A. Varpula, S. Laakso, T. Havia, J. Kyynarainen, M. Prunnila, Harvesting vibrational energy using material work functions, Scientific Reports 4 (2014) 6799. doi:10.1038/srep06799.

[4] J. Davidson, C. Mo, Recent advances in energy harvesting technologies for structural health monitoring applications, Smart Materials Research 2014 (ID 410316) (2014) 1–14. doi:10.1155/2014/410316.

[5] A. Mitura, K. Kecik, J. Warminski, W. Jarzyna, S. Lenci, A numerical study of an autoparametric system with electromagnetic energy harvester, Proceedings of the ECCOMAS Thematic Conference on Multibody Dynamics 2015 (June 29–July 2, 2015) 609–615. doi:978-84-944244-0-3.

[6] K. Kecik, M. Borowiec, An autoparametric energy harvester, European Physical Journal - Special Topics 7 (2013) 1597–1605. doi:10.1140/epjst/e2013-01948-2.

[7] K. Kecik, Application of shape memory alloy in harvesto-absorber system, Acta Mechanica et Automatica 9 (3) (2015) 155–160. doi:10.1515/ama-2015-0026.

[8] A. Jonnalagadda, Magnetic induction systems to harvest energy from mechanical vibrations, Master of Science in Mechanical Engineering, Massachusetts Institute of Technology (2007) 1–108.

[9] D. Barton, S. Burrow, L. Clae, Energy harvesting from vibrations with a nonlinear oscillator, Journal of Vibration and Acoustics, Transactions of the ASME 132 (2) (2010) 0210091–0210097. doi:10.1115/1.4000809.

[10] B. Joyce, Development of an electromagnetic energy harvester for monitoring wind turbine blades, M.S. thesis, Virginia Polytechnic Institute and State University (2011) 1–111.

[11] B. Mann, N. Sims, On the performance and resonant frequency of electromagnetic induction energy harvesters, Journal of Soundand Vibration 329 (1-2) (2010) 1348–1361. doi:10.1016/j.jsv.2009.11.008.

[12] B. Mann, N. Sims, Energy harvesting from the nonlinear oscillations of magnetic levitation, Journal Sound and Vibration 319 (2009) 515–530. doi:h10.1016/j.jsv.2008.06.011.

[13] A. Bernal, L. Garcia, The modelling of an electromagnetic energy harvesting architecture, Applied Mathematical Modelling 36 (10) (2012) 4728–4741. doi:10.1016/j.apm.2011.12.007.

[14] A. Munaz, B. Lee, G. Chung, A study of an electromagnetic energy harvester using multi-pole magnet, Sensors and Actuators A: Physical 201 (2013) 134–140. doi:10.1016/j.sna.2013.07.003.

[15] S. Beeby, M. Tudor, N. White, Energy harvesting vibration sources for microsystems applications, Measurement Science and Technology 17 (12) (2006) R175. doi:http://stacks.iop.org/0957-0233/17/i=12/a=R01.

[16] C. Williams, R. Yates, Analysis of a micro-electric generator for microsystems, Sensors and Actuators A: Physical 52 (1-3) (1996) 8–11. doi:10.1016/0924-4247(96)80118-X.

[17] P. Mitcheson, T. Green, E. Yeatman, A. Holmes, Architectures for vibration-driven micropower generators, Journal of Microelectromechanical Systems 13 (3) (2004) 429–440. doi:10.1109/JMEMS.2004.830151.

[18] N. Stephen, On energy harvesting from ambient vibration, Journal of Soundand Vibration 293 (1-2) (2006) 409–425. doi:10.1016/j.jsv.2005.10.003.

[19] A. Mitura, K. Kecik, Influences of system parameters on energy harvesting from autoparametric absorber, Vibration in Physical Systems 27 (2016) 287–292.

[20] R. Olaru, R. Gherca, C. Petrescu, Analysis and design of a vibration energy harvester using pernament magnets, Revue Roumaine des Sciences Techniques - Serie Electrotechnique 59 (2) (2014) 131–140.

[21] V. Bedekar, J. Oliver, S. Priya, Pen harvester for powering a pulse rate sensor, Journal of Physics D: Applied Physics 42 (10) (2009) 105105. doi:10.1088/0022-3727/42/10/105105.

[22] R. Bobryk, D. Yurchenko, On enhancement of vibration based energy harvesting by a random parametric excitation, Journal of Sound and Vibration 366 (2016) 407–417. doi:10.1016/j.jsv.2015.11.033.

[23] A. Guthrie, A. Frolenkov, J. Mur-Miranda, Limit behavior of the magnetic coupling coefficient for mid–range, near–field applications, Journal of Physics: Conference Series 476 (2013) 012116. doi:0.1088/1742-6596/476/1/012116.

[24] L. Zuo, B. Scully, J. Shestani, Y. Zhou, Design and characterization of an electromagnetic energy harvester for vehicle suspensions, Smart Materials and Structures 19 (4) (2010) 045003. doi:10.1088/0964-1726/19/4/045003.

[25] P. Wang, K. Tanaka, S. Sugiyama, X. Dai, X. Zhao, J. Liu, A micro electromagnetic low level vibration energy harvester based on mems technology, Microsystem Technologies 15 (2009) 941–951. doi:0.1007/s00542-009-0827-0.

[26] E. Doedel, B. Oldeman, Auto-07p: Continuation and bifurcation software for ordinary differential equations, Concordia University, Montereal (2012) 1–266.